ELSEVIER

Journal of Power Sources 52 (1994) 223–229

JOURNAL OF POWER SOURCES

Reactions during reversal of an Ni–H_2 cell ☆

Hari Vaidyanathan [a], Gopalakrishna M. Rao [b]

[a] *COMSAT Laboratories, Clarksburg, MD 20871-9475, USA*

[b] *NASA Goddard Space Flight Center, Greenbelt, MD 20771, USA*

Received 10 March 1994; in revised form 8 August 1994; accepted 19 August 1994

Abstract

The chemical reactions that occur during reversal of aerospace-design nickel–hydrogen (Ni–H_2) cells are examined by determining voltage changes and heat dissipation. Radiative calorimetry is used to measure the rate of heat dissipation during charge, discharge, and reversal. The heat dissipated during reversal at C/10 rate (8.1 A) for a positive precharge cell is four times greater than that for a hydrogen precharge cell. For a cell design with a positive precharge, the reversal reactions consist of completion of nickel electrode discharge and hydrogen evolution on the nickel (positive) electrode, platinum oxide/hydroxide formation, and subsequent reduction by hydrogen at the hydrogen (negative) electrode.

Keywords: Nickel–hydrogen cells; Reversal reactions

1. Introduction

The nickel–hydrogen (Ni–H_2) battery is considered to be robust for aerospace applications, especially for spacecraft with power requirements greater than 1 kWh. Furthermore, this battery was chosen for several existing low-earth-orbit and geosynchronous satellites because of its high usable specific energy and very long cycle life. This electrochemical system has been examined in detail [1–5] to define its performance features and to identify the design parameters that influence its reliability and life expectancy. Some of the conclusions drawn from these studies support earlier assertions regarding a specific energy of 60 Wh kg^{-1}, the dominant role of the positive plate structure in controlling cell performance, and the effect of KOH concentration on capacity [6] and cycle life. A new concern was also raised regarding the impact of increased depth-of-discharge cycling of multicell batteries on reliability and life expectancy. This concern arises from an inadequate understanding of heat dissipation and reversal reactions when one cell in a multicell assembly reverses during routine, high depth-of-discharge cycling.

Heat dissipation during charge/discharge has been examined by several researchers [7,8]. The present study focuses on heat dissipation and chemical reactions during reversal of Ni–H_2 cells.

2. Experimental

Radiative calorimetry was employed to measure heat dissipation from Ni–H_2 cells, in order to determine the electrochemical and thermal characteristics of the cells during reversal. This approach is especially well suited to this task, for the following reasons:

- it is more accurate than conductive calorimetry
- since the $mC_p\,dT/dt$ term is involved in the calculation, the technique is ideal for transient measurements
- the apparatus is simple, consisting of a copper chamber in a vacuum. The measurement technique is automated and incorporates protective features for the cell, using temperature, voltage, and pressure sensors that work in conjunction with relays and electronic circuitry

Lightweight flight-model Ni–H_2 cells, one manufactured by Gates Aerospace Batteries (GAB) and the other by Eagle Picher Industries (EPI), were used in this study. The cells were of aerospace design, consisting of sintered, electrochemically impregnated positive electrodes and platinum catalyst negative electrodes in-

☆ This paper is based on work performed at COMSAT Laboratories under the joint sponsorship of COMSAT Corporation and the National Aeronautics and Space Administration (NASA) Goddard Space Flight Center.

0378-7753/94/$07.00 © 1994 Elsevier Science S.A. All rights reserved
SSDI 0378-7753(94)02011-Q

terleaved with a separator and arranged in a cylindrical Inconel pressure vessel. The cells were procured by the National Aeronautics and Space Administration (NASA) and made available for this study by Goddard Space Flight Center. They were rated at 81 Ah. The major differences between the two cells were that the GAB cell used two layers of Zircar separator and a recirculating stack configuration, while the EPI cell used one layer of asbestos and one layer of Zircar, with a back-to-back stack configuration. Both cells were believed to be negative-limited by design.

In preparing the cells for calorimetry, great care was taken that each cell had a distinct radiating surface. Fourteen thermocouples were installed on the cell canister, and thermofoil heaters were placed within the cylindrical part of the cell. The dome and terminal areas were insulated by wrapping with multiple layers of aluminized Mylar. The thermocouple sensor wires, terminal leads, strain gage input and output leads, and cell voltage sensor leads were bunched to create two thermally insulated wire bundles, with thermofoil heaters to maintain the bundles at a predetermined temperature. Fig. 1 is a schematic diagram of a cell prepared for calorimetry.

The radiative calorimeter consists of a 0.5 m^3 copper chamber that is maintained at −168 °C by circulating liquid nitrogen. The inside of the chamber is painted black, and two thermocouples monitor the interior temperature. A cell is installed in the calorimetric chamber by suspending it with a lacing cord. The calorimetric chamber is arranged in a bell-jar-type vacuum chamber, and a vacuum of 10^{-5} torr is maintained.

Radiative calorimetry is conducted under non-isothermal conditions. The calorimeter functions by creating a condition in which radiation is the mode of heat transfer from the Ni–H_2 cell to the surroundings.

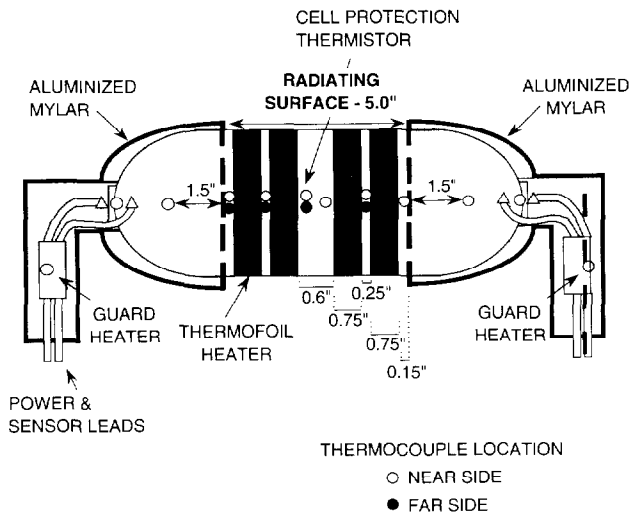

Fig. 1. Schematic of the Ni–H_2 cell prepared for calorimetry. Thermocouple location: (○) near side; (●) far side.

Heat is applied to the cell through the thermofoil heaters to raise the cell temperature significantly above that of the calorimetric chamber, which is maintained at −168 °C. Thus, heat is radiated from the cell at all times and follows the relationship:

$$q = E\sigma(T_c^4 - T_s^4) \quad (1)$$

where E = emissivity; σ = Stefan–Boltzmann constant; T_c = temperature of the cell; T_s = temperature of the calorimeter.

The first step in calorimetry is calibration, which is accomplished by obtaining steady-state temperatures for the cell in the open-circuited condition for different amounts of heat (W) applied through the thermofoil heaters. Then, an equation is derived to relate the average temperature of the cell to the heat radiated, q_r, in W, assuming that the heat applied is radiated out. The thermal capacity of the cell was determined from transient warm-up and cool-down curves and the measured q_r. The general equation used to calculate heat dissipation is:

$$mC_p\, dT/dt = q_d + q_{heater} - q_r \quad (2)$$

where m = mass of the Ni–H_2 cell (g); C_p = thermal capacity of the cell (J °C $^{-1}$); T = average temperature of the cell (°C); t = time (h); q_d = heat liberated from the cell (W); q_{heater} = heat applied to the thermofoil heater tape, current × volt (W); q_r = heat radiated from the cell (calorimetric calibration) (W).

The average temperature of the cell is provided by eight thermocouples installed on the radiating surface of the cell (the area covered by the heater tape). Differences in the eight thermocouple readings were less than 0.1 °C. The test parameters and calculated values are given in Table 1.

3. Results of calibration

Steady-state measurements of the cell temperature at different values of cell heater power yielded a linear relationship. Based on the assumption that all heat from the cell is radiated, the following equation was formulated to calculate the heat radiated, q_r:

EPI cell: $$q_r = 9.32417 + 0.13129T + 0.00068T^2 + 0.00004T^3 \quad (3a)$$

GAB cell: $$q_r = 8.88868 + 0.13431T + 0.00075T^2 + 0.00001T^3 \quad (3b)$$

where q_r is the heat radiated and T is the temperature of the cell (average of eight thermocouples readings).

Next, the thermal capacity of each cell was determined from the temperature transients (warm-up) obtained at a heater power of 8.7 W for the GAB cell and

Table 1
Test parameters

Item	Value
Cell mass	EPI cell = 2211 g; GAB cell = 2103 g
Calorimetric temperature	−168 °C
Calorimetric pressure	10^{-5} torr
Heat transfer mode	Radiation
Cell temperature	Average of the eight thermocouples located on the radiating surface of the cell. Cell temperature varies from −5 to 35 °C during charge/discharge
Radiating surface	156 cm^2
Heater power required to maintain cell at 10 °C	EPI cell = 10 W; GAB cell = 9.6 W

8.13 W for the EPI cell for 12 h. The cell temperatures obtained at several time intervals were converted to q_r using the calibration equation, and the thermal capacities of the GAB and EPI cells were calculated to be 2200 and 2005 J $°C^{-1}$, respectively. Thus, the specific heats of the cells are 0.9533 and 0.995 J $(°C\ g)^{-1}$ for the GAB and EPI cells, respectively. These values were compared with values obtained by summing the specific heats of the various cell components (e.g., KOH, platinum negative electrode, Inconel cell canister, nickel tabs, and positive plates) and agreement within 5% was obtained.

An error analysis was performed which took into consideration errors in temperature measurement, heat leakage through the Mylar insulation, curve fitting, heater power, guard heater operation, and cell thermal capacity. The root-sum-square error was calculated to be 0.055 W.

4. Heat dissipation during charge and discharge

The cell was charged at a constant current of 8.1 A for 16 h, and then discharged at a constant current of 40 A until the cell voltage reached 0.1 V. The power to the thermofoil heater was adjusted to 9 W and held constant throughout the charge/discharge cycle. The test conditions were non-isothermal, and the cell temperature varied with time, which directly reflected the magnitude of the endothermic and exothermic reactions occurring inside the cell.

Fig. 2 shows the voltage and heat dissipation profiles during charge and discharge for the EPI cell. The voltage profile (Fig. 2(a)) resembles the behavior generally observed in Ni–H_2 cells and is characterized by an overcharge region in which the voltage change is minimal. It exhibits an end-of-charge voltage of 1.50 V and a discharge voltage profile containing a single major plateau with an average discharge voltage of 1.23 V. The heat dissipation profile (Fig. 2(b)) is characterized by an initial exothermic heat of 0.3 W, which decreases, becomes slightly endothermic, and then remains in a state of minimum heat generation for 10

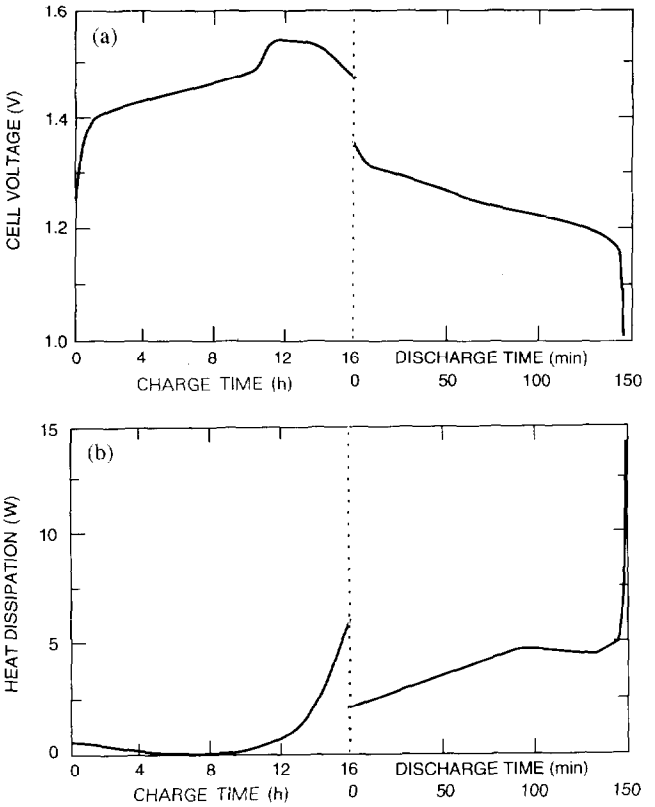

Fig. 2. Profiles for the EPI cell during charge/discharge at 0 °C: (a) voltage; (b) heat dissipation.

h. The initial exothermic heat is attributed to the nickel precharge design, in which the cell contains no hydrogen gas at the end of discharge (or beginning of charge). Heat produced by the reaction of traces of oxygen with hydrogen to form water accounts for the first episode of exothermic heat. Contrary to common belief, endothermic cooling was found to be insignificant during charge.

After about 10 h of charging, there was a marked increase in heat dissipation and, since this was a non-isothermal test, the cell temperature increased to 35 °C. In the case reported here, the cell was allowed to cool to 0 °C by open-circuiting it and cutting off the heater power for 1 h prior to discharge. The heat

Table 2
Comparison of heat dissipation

Item	EPI cell	GAB cell
Average heat rate during 16 h charge at 8.1 A at 0 °C (W)	0.55	3.61
Average heat rate during discharge at 40 A at 0 °C (W)	7.9	9.96
Average heat rate in one charge/discharge cycle (W)	1.36	4.55
Thermal capacity (J °C^{-1})	2005	2200

dissipation rate during discharge increases slowly until about 50% of the stored energy has been removed, levels off for a brief period, and then increases rapidly with subsequent increase in cell temperature. The voltage and heat dissipation profiles shown in Fig. 3 for the GAB cell exhibit the same general trends as for the EPI cell, except for the heat dissipation rate, which increases slowly until 20% of the energy has been removed, levels off for a long period, and then increases rapidly.

Differences in the magnitude of heat produced by the two cells are recorded in Table 2. The temperature of 0 °C referred to in the Table indicates the temperature at the beginning of charge/discharge. As mentioned earlier, the cell temperature is allowed to increase or decrease, depending on internal reactions.

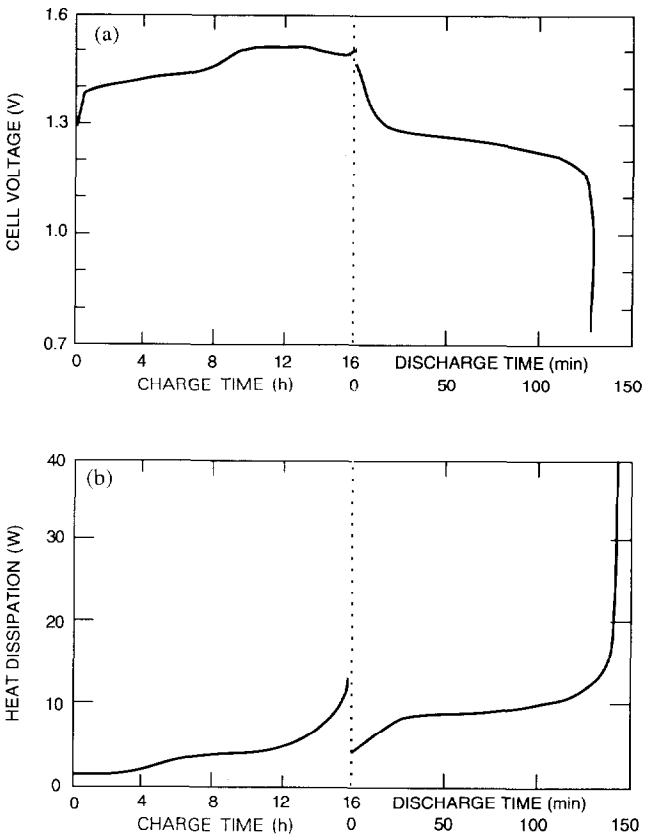

Fig. 3. Profiles for the GAB cell during charge/discharge at 0 °C: (a) voltage; (b) heat dissipation.

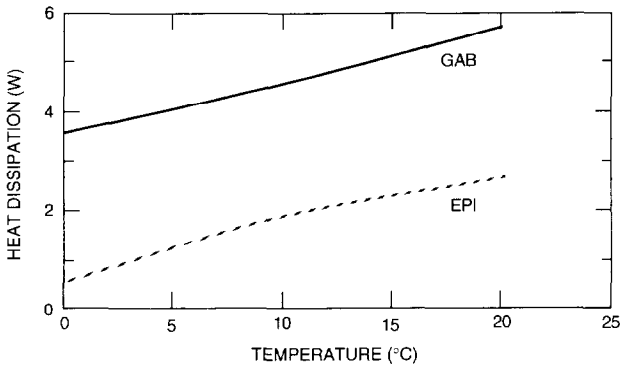

Fig. 4. Heat dissipation on charge at 8.1 A at different initial temperatures.

The data indicate a marked difference in heat dissipation for the two cells, despite common design features such as sintered electrochemically impregnated positives, platinum anode catalyst, 31% KOH as electrolyte, and Zircar separator. The higher heat rate in the GAB cell is attributed to higher polarization of the positive plate, which results in parasitic oxygen evolution. Oxygen reacts with hydrogen, producing heat. The occurrence of parasitic reactions can be discerned from data obtained for heat dissipation at different initial charge temperatures. Fig. 4 shows the average heat dissipation rate during charge at 8.1 A for the GAB and EPI cells at different initial charge temperatures. For both cells, the cell heat dissipation increases with increasing temperature, as expected. It is well known that the fraction of the charging current that generates oxygen increases with increasing temperature. Here again, the GAB cell dissipates more heat than the EPI cell.

5. Cell reversal tests

These tests were performed in the following steps:
Step 1. Stabilize the cell at 10 °C by adjusting the heater power supplied to the cell.
Step 2. Charge at 8.1 A for 16 h.
Step 3. Discharge at 40 A until 0.1 V.
Step 4. Discharge the cell at different currents (reversal).
Step 5. Measure steady-state cell voltage and heat dissipation.

Again, the cell temperature was allowed to rise or fall during the test. The reversal current was 8.1 A at the beginning of the test, and the voltage stabilized in 70 min for the EPI cell and 380 min for the GAB cell. Subsequent reversals at higher currents required less time for voltage stabilization, with the time being limited to less than 30 min for the reversal at 40 A.

6. Voltage and heat rate during reversal

The voltage and heat rate were monitored continuously during reversal. Fig. 5 shows the variation in heat dissipation with time at different reversal currents for the EPI and GAB cells. At constant currents of 8.1, 16, and 40 A, the data show that negative voltage increased with time until a steady value was attained. At a reversal current of 8.1 A, the cell voltages were −1.645 V for the EPI cell and −0.054 V for the GAB cell. There is a marked difference in the magnitude of reversal voltages at all reversal currents for the two cells studied, with the EPI cell exhibiting more negative voltages during reversal. The reversal voltages were plotted against the logarithm of current, as shown in Fig. 6. The EPI cell exhibited a linear relationship (Fig. 6(a)), while the GAB cell showed a nonlinear

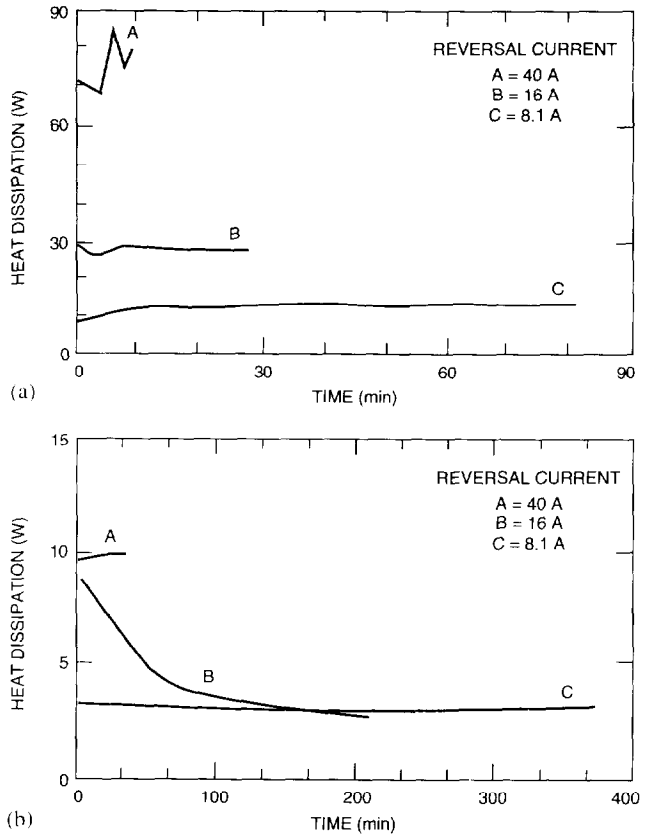

Fig. 5. Variation of heat dissipation during reversal at constant current: (a) EPI cell; (b) GAB cell.

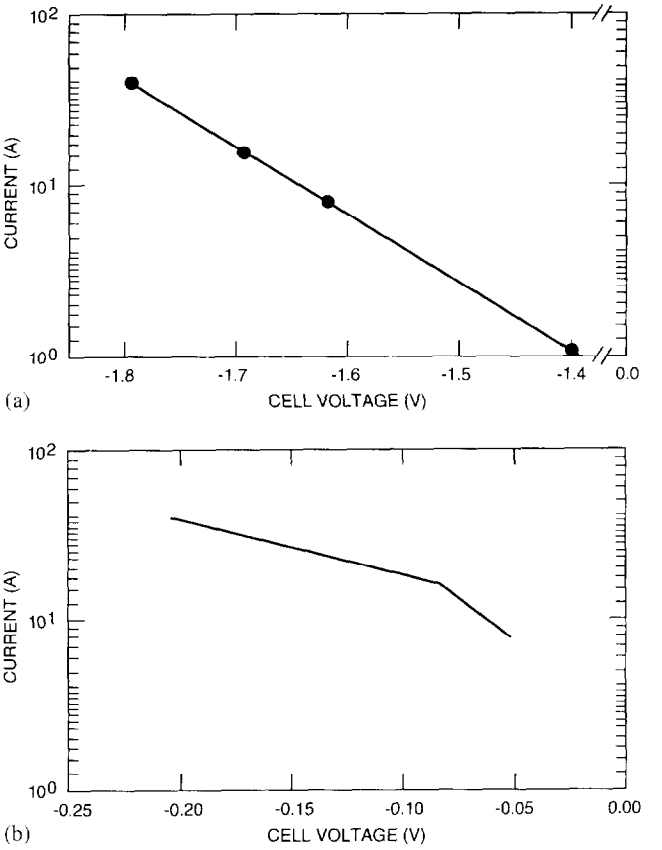

Fig. 6. Variation of cell reversal voltage with reversal current at 10 °C: (a) EPI cell; (b) GAB cell.

relationship (Fig. 6(b)). Heat dissipation for the EPI cell is much higher than for the GAB cell. For example, at 40 A reversal ($C/2$ rate), the heat dissipation from the EPI cell is 71.9 W, compared to 12.52 W for the GAB cell.

7. Mechanism of reversal

The reversal voltages can be used to formulate a sequence for the electrochemical reactions that occur during reversal. The EPI cell reverses at −1.4 V at a current of 1.2 A, which is 4.16×10^{-4} A cm^{-2}. At this rate of reversal, the measured heat production is 1.74 W, which is close to the value obtained when the current is multiplied by the reversal voltage. The reactions at the nickel positive electrode consist of completion of nickel electrode discharge and hydrogen evolution, which occurs at −0.94 V according to:

$$NiOOH + H_2O + e^- \longrightarrow Ni(OH)_2 + OH^-$$

$$H_2O + e^- \longrightarrow H + OH^-$$

$$2H \longrightarrow H_2$$

The corresponding reaction at the platinum negative electrode is expected to be oxygen evolution, which

involves intermediate chemical steps of platinum oxidation, formation of platinum hydroxide, dehydration of the hydroxide, and growth of oxide film, as follows:

$$Pt + OH^- \longrightarrow PtOH + e^-$$

$$PtOH + OH^- \longrightarrow Pt(OH)_2 + e^-$$

$$Pt(OH)_2 \longrightarrow PtO + H_2O$$

$$Pt(OH)_2 \longrightarrow Pt + H_2O + O$$

$$O + O \longrightarrow O_2$$

Oxygen reaction on platinum has been studied by several authors [9,10] who have reported that the Tafel parameters change with increasing voltage, and that oxide film growth occurs. Streibel et al. [11] have shown by cyclic voltammetry that in 6.9 M KOH, the oxide formation region on platinum falls between 0.46 and 1.4 V and is indicated as a precursor for oxygen evolution. During reversal, platinum is anodized and oxide film grows on the surface. Since the Ni–H_2 cell used an electrode and stack design that facilitates gas transport, hydrogen diffuses readily toward the platinum electrode and reacts with the Pt(O) or $Pt(OH)_2$ film on the negative electrode to produce water. The reactions can be symbolized as:

$$PtO + H_2 \longrightarrow Pt + H_2O$$

$$Pt(OH)_2 + H_2 \longrightarrow Pt + 2H_2O$$

The reaction on platinum does not develop into oxygen evolution, but only into oxide/hydroxide formation. Thus, at low current densities, the oxide/hydroxide film is reduced by hydrogen gas before the reaction progresses to oxygen evolution. The reversal reactions can be summarized as follows:

- completion of nickel electrode discharge
- hydrogen evolution on nickel
- oxide film formation on platinum
- recombination of hydrogen with PtO species to form water

Thus, oxygen evolution is not induced by a reversal voltage of −1.40 V, and the pressure sensor did not register any increase in cell pressure. It is unclear whether the platinum species that reacts with hydrogen is an oxide or hydroxide.

The reversal voltage increases with current due to polarization of the hydrogen-evolution reaction on nickel, and platinum oxide reduction at the platinum electrode. The Tafel-type plot shown in Fig. 6(a) represents the variation of the mixed potential with current. Since the oxide reduction/hydrogen oxidation is more prone to polarization, the increase in reversal voltage with current is more attributable to the reactions at the platinum electrode. At high rates of reversal (40 A), the sequence of reactions is expected to progress to O_2 evolution.

8. Reversal reactions of the GAB cell

The reversal voltage of the GAB cell is −0.054 V at a current density of 2.81 mA cm^{-2}, and does not increase with current density as in the case of the EPI cell. The GAB reversal voltage can be explained by hydrogen generation and oxidation reaction, as follows:

(i) nickel electrode:

$$H_2O + e^- \longrightarrow H + OH^-$$

$$2H \longrightarrow H_2$$

(ii) platinum electrode:

$$H_2 \longrightarrow H + H$$

$$H + OH^- \longrightarrow H_2O + e^-$$

The hydrogen evolution on nickel in the 31% KOH used in the cell is polarized and occurs at about −0.94 V. The hydrogen oxidation reaction at a current density of 2.81 mA cm^{-2} (determined by independent testing in a polarization cell) occurs at −0.89 V on platinum in 31% KOH. Thus, this cell behaves like a hydrogen precharged cell. The small increases in reversal voltage with current density are attributable to low polarization of the hydrogen oxidation reaction on platinum, and hydrogen evolution on nickel.

9. Conclusions

The results of this study indicate a truly negative-limited condition for the EPI cell. The GAB cell behaved like a positive-limited cell. In a negative-limited cell, the reversal reactions are completion of nickel electrode discharge and hydrogen evolution on the nickel positive electrode, oxide/hydroxide formation on the platinum negative electrode, and the reduction of platinum oxide/hydroxide by hydrogen to form water.

In the positive-limited (GAB) cell, hydrogen evolution at the nickel electrode and hydrogen oxidation at the platinum electrode occur during reversal. The negative-limited cell dissipated four times more heat than the positive-limited cell during reversal.

The observation of higher heat dissipation in a negative-limited cell is an important finding that implies that reversal at high currents will result in very high heat radiation in a space environment. Reversal at high current, occurring within a weak cell in a battery pack during discharge, would raise the battery temperature beyond the limits for which it was designed. This prompts concern about the use of nickel precharge, since perfect cell matching is a requirement, especially in applications where the depth-of-discharge is very high.

Acknowledgements

The authors wish to thank NASA Goddard Space Flight Center for permission to publish this work. They also gratefully acknowledge the help of R. Clark and W.H. Kelly in performing the calorimetry.

References

[1] D.D. Mcdonald and M.L. Challingsworth, *J. Electrochem. Soc., 140* (1993) 606.
[2] A.H. Zimmerman, *Proc. Symp. Nickel Hydroxide Electrodes,* Proc. Vol. 90-4, The Electrochemical Society, Pennington, NJ, 1990, p. 311.
[3] J. Kim, T.V. Ngyuen and R.E. White, *J. Electrochem. Soc., 139* (1992) 2781.
[4] A. Visintin, S. Srinivasan, A.J. Appleby and H.S. Lim, *J. Electrochem. Soc., 139* (1992) 985.
[5] H. Vaidyanathan and K. Burch, *Proc. Intersociety Energy Conversion Engineering Conf., Reno, NV, USA, 1990,* American Institute of Chemical Engineers, New York, NY, Vol. 6, p. 69.
[6] H.S. Lim and S.A. Verzwywelt, *J. Power Sources, 22* (1988) 213.
[7] C.J. Johnson, *Ext. Abstr., Fall Meet. of The Electrochemical Society, Pennington, NJ, USA, 1989,* Abstr. No. 36.
[8] H. Vaidynathan and W.H. Kelly, *Proc. Intersociety Energy Conversion Engineering Conf., San Diego, CA, USA, 1992,* Society of Automobile Engineers, Warrendale, PA, Vol. 1, p. 209.
[9] V.I. Birss and A. Damjanovic, *J. Electrochem. Soc., 134* (1987) 113.
[10] A. Damjanovic and P.G. Hudson, *J. Electrochem. Soc., 135* (1988) 2269.
[11] K.A. Streibel, F.R. McLarnon and E.J. Cairns, *J. Electrochem. Soc., 137* (1990) 3351.